CFSRC COLLOQUIUM

Proceedings of the Cold-Formed Steel Research Consortium Colloquium
20-22 October, 2020 (cfsrc.org)

Metal Building Roof Purlin Line Strength by Computation

Cristopher D. Moen[1]

Abstract

A computation-based method for metal building purlin and girt design is introduced using the AISI S100-16 North American Specification for the Design of Cold-Formed Steel Structural Members. Purlin section properties, span length, material properties, and boundary conditions, including bracing connectivity to exterior screw-fastened or standing seam panels, are defined. Flexure, shear, and torsional strengths are calculated along the line. The capacity of the roof or wall system is determined by applying a gravity or uplift load until a strength limit state is reached. For uplift loads, buckling deformation of the purlin free flange between intermediate bridging is considered. The calculations are performed with an open-source software package called StructuresKit.jl written in the Julia computing language. Predicted strengths from the calculation method are compared to the experimentally determined strengths from 49 simple span Cee and Zee wall girt line uplift pressure box tests, some of which were constructed with rigid board insulation.

1. Introduction

This paper presents a method for calculating the strength of a metal building roof purlin or girt line using AISI S100-16 *North American Specification for the Design of Cold-Formed Steel Structural Members*. A new Section I6.1 was added to the Specification in 2016 that provides instructions for calculating purlin line strength as an alternative to pressure box testing. In the method, an engineer calculates the demand loads and limit state strengths (e.g., shear+flexure interaction, distortional buckling) along the line considering bracing connectivity from screw-fastened or standing seam roof or wall panels, from intermediate bridging, and insulation.

Even with a well-defined procedure, accurately predicting the behavior and strength of a purlin line by calculation is still challenging. The pressure from the roof concentrates on the connected purlin flange, and the loading point is far from the cross-section shear center, which creates a torsion. Some of this torsion is taken in the roof or wall panel, some of it goes into the purlin. There can be purlin cross-sectional deformation from local buckling and distortional buckling. For gravity loads, the purlin compression flange is partially braced by the connection to the roof panel and there is a lateral load component if the roof is sloped. Cross-sectional deformation of the compressed free flange can dominate the system capacity when restrained flexural-torsional buckling combines with shear flow accumulating in the flange, especially if there is no intermediate bridging. All of these should be considered in a calculation-based method.

Thanks to research investment over the past 60 years from the cold-formed steel and metal building industries, most of these calculation challenges have been addressed. Capacity calculation of thin-walled cold-formed steel members considering system connectivity is convenient and accurate with the Direct Strength Method [1], and the use of the Direct Strength Method has been confirmed as a viable strength prediction approach for girts and purlins, e.g. [2] and [3] if cross-sectional deformation from buckling and shear flow in the cross-section is considered ([4],[5], [6]). Stiffness characterization of the connections between purlins and screw-fastened [7] and standing seam roofs [8] provides useful values for a purlin line strength calculation considering system bracing. Structural analysis considering global deformations of purlin lines including load eccentricities and system connectivity can be performed without much trouble, e.g., [9] or [10]. So what next then? In the following sections a calculation workflow that includes much of this research is organized and automated with open-source software.

2. StructuresKit.jl

As you read through the research literature on metal building purlin strength prediction, you will find a good bit has been supported by software, even looking back 30 or 40 years ago. This shouldn't be surprising, especially considering the long list of system details described in the previous section that needs to be considered. The computation method described

[1]Owner, RunToSolve, LLC, cris.moen@runtosolve.com

herein is again enabled software, in this case as the open-source package StructuresKit.jl.

StructuresKit.jl is written in the Julia scientific computing language and within StructuresKit.jl, there are modules like AISIS10016 that automate all the Direct Strength Method equations need to define the strength limit states. The module Beam calculates the purlin line deformations including bracing connectivity and load eccentricities with second order analysis. BeamColumn is used to approximate cross-section deformation of an unbraced free flange. And from these deformations, the module InternalForces calculates moments, shear, torsion, and bimoment that represent the demands along the purlin line. The module CrossSection is used to calculate section properties. And there is PurlinDesigner , the wrapper module that uses all of these tools to load a purlin line to failure, thus defining its available strength, strength limit state, and failure location along the line.

Documentation, examples, and a testing validation log for StructuresKit.jl are available on Github. For those of you who are wondering why Julia, it was chosen over other languages (e.g., Python or Matlab) because (1) its package manager makes it convenient to write, organize, and distribute code; (2) it is open-source with an active, positive, and helpful developer community; and (3) it has fast, efficient, native nonlinear solvers and tools for solving systems of differential equations that were needed in this application.

3. Definition of the Purlin Line

The purlin line strength calculation with StructuresKit.jl begins by defining section properties, i.e., Section Properties = [(Ix1, Iy1, Ixy1, Cw1, Wn1, Mcrlxx1, Mcrlyy1), (Ix2, Iy2, Ixy2, Cw2, Wn2, Mcrlxx2, Mcrlyy2),...]. More than one cross-section type can be listed as shown. The critical elastic buckling moments $Mcr\ell xx$ and $Mcr\ell yy$ about the purlin centroidal axes shown in Figure 1 can be calculated with your favorite thin-walled elastic buckling program (e.g., Thin-Walled 2 [11], GBTUL [12], CUFSM [13], CFS). Here they are determined with a Python translation of CUFSM called pyCUFSM. The cross-section maximum normalized warping stress W_n is calculated using StructuresKit.CrossSection with a translation of the function cutwp_prop2.m from CUFSM to Julia.

The purlin cross-section dimensions are defined as CrossSectionDimensions = [(t1, ho1, b1, d1, 1, CorZ1, h1, c1), (t2, ho2, b2, d2, 2, CorZ2, h2, c2), ... where t is the base metal thickness, h_o, b, and d are the out-to-out web depth, flange width, and lip length respectively, θ is the flange lip angle in degrees measured from the horizontal, CorZ=0 for a Cee section, CorZ=1 for a Zee section, h is the flat web width, and c is the distance from centerline of the flange-to-roof panel connection to purlin center of twist defined in Fig. 2 of [2]. The LoadLocation = (ax1, ay1),(ax2, ay2),... where a_x and a_y are the x and y distances from the load to the cross-section shear center in the centroidal axis coordinate system. MaterialProperties=[(E1, ν1, Fy1),(E2, ν2, Fy2),...] where E is the elastic modulus, ν is Poisson's ratio, and F_y is the steel yield stress. Bracing and connectivity are defined as BracingProperties = [(kx1, kphi1, Lm1, a1),(kx2, kphi2, Lm2, a2),...], where k_x and k_ϕ are the translational and rotational distributed stiffnesses provided by the roof or wall panel's connectivity to the purlin. The length of discrete distortional buckling restraint is L_m and a is the shear stiffener spacing if they are provided.

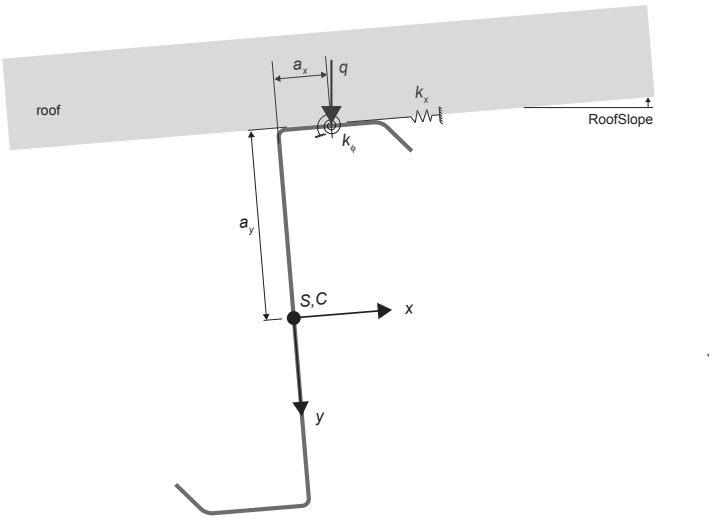

Figure 1: Purlin connected to a roof panel

The purlin line is defined from left to right in member groups as MemberDefinitions = (L1, dL1, 1, 2, 1, 2), (L2, dL2, 1, 1, 1, 1),..., where L is the length of a member group and dL is the length of the group discretization. (The number of segments within a member group affects the accuracy of the structural analysis.) The four numbers after dL are the SectionProperties, MaterialProperties, CrossSectionDimensions, and BracingProperties assigned to each member group. An example of a multi-span purlin line in StructuresKit.PurlinDesigner was recently developed for the American Iron and Steel Institute, including a video tutorial.

The system geometry definitions complete the inputs for StructuresKit. The support locations are defined as distances from the left end of the purlin line in Supports, i.e., Supports = [0 7648 7648*2] for a two span line. The far left and far right ends of the purlin line should be defined as simply-supported (1), fixed (2), or free cantilever (3) with EndBoundaryConditions, i.e., EndBoundaryConditions = [1 1] when simply-supported on both ends. The roof slope is defined as RoofSlope, e.g., RoofSlope = 4.76 in degrees. In-

termediate bridging (also sometimes called torsion bracing) locations are defined as distances from the left end of the purlin line as Bridging, i.e., Bridging = [1000 2000 3000 4000 5000].

For all inputs listed above, use consistent units, i.e., kN and m or kips and in.

4. Calculating Purlin Line Strength

Strength limit states are calculated along the purlin line and compared to demand loads with interaction checks. The local buckling strengths $M_{n\ell xx}$ and $M_{n\ell yy}$ are calculated with AISI S100-16 Section F3.2.1. Since global buckling deformations are considered in the second-order analysis, the critical elastic global buckling moment M_{cre} (lateral torsional buckling) is not calculated and it is assumed that $M_{ne} = M_y$. It turns out that M_{cre} does not exist in a meaningful way for this calculation anyway because of the load eccentricities that cause the purlin line to start deforming as soon as it is loaded [9]. The distortional buckling strength M_{nd} is calculated with AISI S100-16 Section F4.1. The shear strength V_n is calculated with AISI S100-16 Section G2.1. The bimoment strength B_n is calculated with a yield limit criterion, i.e., $B_n = C_w * F_y/W_n$.

A uniform load is applied to the purlin line, and a second-order structural analysis is performed to calculate the global deformations and internal forces as the purlin line deflects. Cross-section deformation caused when the purlin has a compressed free flange either from uplift loads or for gravity loads near an interior support is considered in the second order analysis with the methodology described in [2]. The free flange is modeled as a beam-column (flange, lip, and 1/5 of the web) on an elastic foundation using StructuresKit.BeamColumn, where the foundation stiffness is calculated using Eq. 16 of [2] and the shear flow is calculated with Eq. 13a of [2] for a Cee section or Eq. 15 of [2] for a Zee section.

AISI S100-16 limit states and interaction equations are checked along the purlin line at each load step. Combined bending and shear is evaluated with AISI S100-16 Eq. H2-1, combined bending is checked with AISI S100-16 Eq. H1.2, and distortional buckling about the $x-x$ centroidal axis is checked with AISI S100-16 Eq.F4.1-1. Combined bending and torsional load is checked with the interaction equation $\overline{M_x}/M_{ax\ell o} + \overline{M_y}/M_{ay\ell o} + \overline{M_yf}/M_{ayf\ell o} + \overline{B}/B_a \leq 1.15$ where M_x and M_y are the purlin demand moments about the $x-x$ and $y-y$ centroidal axes and M_{yf} is the demand moment on the free flange (flange, lip, and 1/5 of the web) about its $y-y$ centroidal axis caused by cross-sectional deformation. For LRFD, the available local buckling flexural strengths are $M_{ax\ell o} = \phi_b M_{n\ell x}$, $M_{ay\ell o} = \phi_b M_{n\ell y}$ and $M_{ayf\ell o} = \phi_b M_{n\ell yf}$ where $\phi_b = 0.90$ according to AISI S100-16 Section F2. The purlin bimoment demand $\overline{B}$ comes from the second-order structural analysis, and the available bimoment strength $B_a = \phi_t B_n$ where $\phi_t = 0.90$.

The uniform load that results in the first strength limit state or interaction equation to be violated is the purlin line capacity. The capacity can be calculated considering Allowable Stress Design (ASD) or Load Resistance Factored Design (LRFD) or nominal (unfactored) by setting ASDorLRFD = 0 or 1 or 2 respectively.

5. Comparison of Calculations to Experiments

The Metal Building Manufacturers Association (MBMA) sponsored 49 pressure box tests summarized in Table 1 as part of the development of AISI S100-16 I6.1 [14]. The wall girt test series was for simple spans (7468 mm), uplift loading, considering Cee and Zee sections and screw-fastened wall panels. Some of the tests were conducted with fiberglass batting insulation between the purlin and the wall panel, and some were conducted with various thicknesses of rigid board insulation (25mm, 50mm, and 100mm). Intermediate bridging was not included in any of the tests. Measured cross-section dimensions, base metal thickness, and steel material properties are available in [14].

The rotational stiffness of the panel-to-girt connections were also measured experimentally with an F-test setup, see [15] for tests without insulation and [16] for tests with rigid board insulation. The rotational stiffness of the rigid board insulation was taken as the slope of the first leg in Figure 15 of [16], i.e., before the insulation has yielded in compression, which is is consistent with the vacuum box test observations in [14]. The translational stiffness of the panel-to-girt connections without insulation is calculated with the semi-empirical prediction approach in [17]. For tests with rigid board insulation, the translational stiffness with rigid board insulation given in Table 1 is taken as the elastic modulus of the insulation which is approximately 6.7 N/mm^2. This assumes that friction develops between the girt flange and the insulation which is consistent with the test observations. If there is no friction, then the translational stiffness is more or less zero because the fastener cuts through the insulation.

This complete data set, although not so consistent with the multi-span geometry in everyday metal buildings, is useful for showing that the computation method described herein can predict the controlling strength limit state and expected girt line capacity. Dimensions, material properties, and bracing connectivity for the 49 tests are summarized in Table 1 and serves as inputs to StructuresKit.PurlinDesigner. The PurlinSpacing = 2070 mm, the RoofSlope = 0 and L_m=7468 mm (no discrete distortional buckling restraint) and a = 7468 mm (no web shear stiffeners). The span discretization for the second order analysis of each specimen was 200 segments,

i.e., dL = (7468/200) mm. Each simulated test takes about 1 second to run on a 2013 MacBook Pro.

Overall the PurlinDesigner predictions are consistent with the tested vacuum box failure pressures (p_{test} and $p_{predicted}$ in Table 1), with an average test-to-predicted ratio of 1.04 and a coefficient of variation of 0.16. The governing failure mode (in both tests and predictions) was combined strong axis bending, weak axis bending, torsion, and cross-sectional deformation of the free flange. The resulting failure is local yielding, buckling, and folding at midspan near the free-flange web intersection. The PurlinDesigner predictions are more accurate for the Zee section tests. All inputs and Julia code used to perform the 49 analyses are available on Github.

6. Conclusions

A computation-based method for predicting metal building purlin line strength with the AISI S100-16 North American Specification for the Design of Cold-Formed Steel Structural Members is presented. The method utilizes an open source software package StructuresKit.jl that accepts design information about the purlin line and performs a simulated test to collapse in about one second. The method considers many of the structural details in a typical metal building roof system including load eccentricity from the purlin flange to its shear center, roof slope, bracing provided by the roof panel to the purlin including insulation, intermediate bridging, and span arrangement (simple or continuous). Global and cross-section deformations and demand forces, moments, shears, and torsion are obtained along the purlin line with second order structural analysis. The computation-base method consistently predicted the purlin line strengths of 49 simple span uplift tests when all the system details were considered.

References

[1] B. W. Schafer, "Review: The direct strength method of cold-formed steel member design," *Journal of Constructional Steel Research*, vol. 64, 2008. DOI: https://doi.org/10.1016/j.jcsr.2008.01.022.

[2] T. Gao and C. D. Moen, "Extending the direct strength method for cold-formed steel design to through-fastened simple span girts and purlins with laterally unbraced compression flanges," *ASCE Journal of Structural Engineering*, vol. 140, no. 6, 2014. DOI: https://ascelibrary.org/doi/abs/10.1061/(ASCE)ST.1943-541X.0000860.

[3] M. Seek, "Flexural strength of continuous-span z-purlins with paired torsion braces using the direct strength method," 2018.

[4] L. Zetlin, "Unsymmetrical bending of beams with and without lateral bracing," in *Proceedings of the American Society of Civil Engineers*, ASCE, vol. 81, 1955, pp. 1–20.

[5] T. Pekoz and P. Soroushian, "Behavior of c-and z-purlins under wind uplift," in *Sixth International Specialty Conference on Cold-Formed Steel Structures*, 1982.

[6] C. J. Rousch and G. J. Hancock, "Comparison of tests of bridged and unbridged purlins with a non-linear analysis model," *Journal of Constructional Steel Research*, vol. 41, no. 2-3, pp. 197–220, 1997.

[7] T. Gao and C. D. Moen, "Extending the direct strength method for cold-formed steel design to through-fastened simple span girts and purlins with laterally unbraced compression flanges," *ASCE Journal of Structural Engineering*, vol. 140, no. 6, 2014. DOI: https://doi.org/10.1061/(ASCE)ST.1943-541X.0000860.

[8] C. Moen, L. Cronin, and R. Fehr, "Capacity prediction of open-web steel joists partially braced by a standing seam roof," in *2012 Annual Technical Session and Meeting, Structural Stability Research Council, Grapevine, TX*, 2012.

[9] R. Plaut and C. Moen, "Lateral-torsional deformations of c-section and z-section beams with continuous bracing," in *2020 Annual Technical Session and Meeting, Structural Stability Research Council, Atlanta, GA*, 2020.

[10] R. Ziemian and W. McGuire, *Mastan2 v5.1.20*, 2020.

[11] V. Nguyen, G. Hancock, and C. Pham, "Development of the thin-wall-2 program for buckling analysis of thin-walled sections under generalised loading," in *Eighth International Conference on Advances in Steel Structures, Lisbon, Portugal*, 2015.

[12] R. Bebiano, N. Silvestre, and D. Camotim, "Gbtul-a code for the buckling analysis of cold-formed steel members," 2008.

[13] B. W. Schafer and S. Ádány, "Buckling analysis of cold-formed steel members using cufsm: Conventional and constrained finite strip methods," in *Eighteenth International Specialty Conference on Cold-Formed Steel Structures, Orlando, FL*, Citeseer, 2006.

[14] T. Gao and C. D. Moen, "Flexural strength experiments on exterior metal building wall assemblies with rigid insulation," *Journal of Constructional Steel Research*, vol. 81, pp. 104–113, 2013.

[15] T. Gao and C. D. Moen, "Predicting rotational restraint provided to wall girts and roof purlins by through-fastened metal panels," *Thin-Walled Structures*, vol. 61, pp. 145–153, 2012.

[16] T. Gao, "Flexural strength of exterior metal building wall assemblies with rigid insulation," Virginia Polytechnic Institute and State University, Tech. Rep., 2011.

[17] F. Tao, A. Chatterjee, and C. Moen, “Monotonic and cyclic response of single shear cold-formed steel-to-steel and sheathing-to-steel connections,” Virginia Tech Research Report No. CE/VPI-ST-16/01, Blacksburg, VA, Tech. Rep., 2016.

Table 1: Comparison of tested purlin line strength to predicted strength calculated with StructuresKit.PurlinDesigner for a simple span wall girt wind suction (uplift) experimental study [14]

Test number	Test name	Bc mm	Dc mm	θc deg	Bt mm	Dt mm	θt deg	H mm	r mm	t mm	c mm	F_y N/mm^2	$M_{cr\ell,xx}$ N-mm	k_ϕ N-mm/rad/mm	k_x N/mm/mm	p_{test} Pa	$p_{predicted}$ Pa	$p_{test}/p_{predicted}$
2	Z200D-2	68.4	26.4	47	72.5	27.5	53	202	6.6	2.59	39	420	3.22E+07	1491	11.4	790	814	0.97
3	Z200D-3	68.1	25.2	47	65.5	25.7	53	204	8.2	2.54	37	415	2.89E+07	1350	11.0	760	759	1.00
4	Z200B-1	68.6	24.4	47	70.1	28	52	205	7.3	2.57	41	433	3.11E+07	1627	11.8	870	859	1.01
5	Z200B-2W	68	25.8	46	70.1	26.1	53	204	6.7	2.57	36	418	3.06E+07	1287	11.3	890	765	1.16
6	Z250D-1	72	19.8	55	73.3	20.3	46	253	7	1.52	35	403	5.60E+06	1027	6.7	460	412	1.12
7	Z250D-2	72	20.8	55	72.6	21.4	48	253	6.5	1.52	31	401	5.58E+06	858	6.7	450	392	1.15
8	Z250B-1	71.7	21.1	55	72.9	22.1	47	253	5.9	1.51	25	401	5.50E+06	600	6.7	440	353	1.25
9	Z250B-2	70.7	22.3	54	73.3	20.3	47	251	6.1	1.5	42	399	5.37E+06	1274	6.6	480	414	1.16
10	C200D-1	65.2	21.3	90	65	21.7	90	203	5.1	2.57	34	522	5.39E+07	978	15.3	800	740	1.08
11	C200D-2	65.8	21.3	90	64.5	21.3	90	203	5.8	2.57	26	519	5.34E+07	594	15.2	690	544	1.27
12	C250D-1	64.5	20.9	89	65.5	19.6	89	254	5.6	1.49	20	423	9.40E+06	239	7.1	330	212	1.56
13	C250D-2	63.8	20.8	91	65	19.3	91	254	5.5	1.5	21	414	9.53E+06	264	6.9	330	224	1.48
14	Z200D-R100-1	67.9	25.2	48	67.9	27.6	53	205	5.7	2.54	40	428	2.94E+07	1554	11.5	810	829	0.98
15	Z200D-R100-2	67.9	25.6	47	67.9	26.5	52	205	6.3	2.51	21	418	2.81E+07	457	11.0	470	443	1.06
16	Z200D-TH25-1	70.6	25.3	46	70.8	28	52	204	7.1	2.54	37	428	2.98E+07	1048	6.7	770	684	1.13
17	Z200D-TH25-2	66.1	26.3	47	69.4	26.3	53	205	6.3	2.54	45	418	2.96E+07	1362	6.7	820	786	1.04
18	Z200D-TH50-1	73.3	24.1	48	69.3	26.2	53	202	7.7	2.57	37	423	3.02E+07	1514	6.7	850	783	1.09
19	Z200D-TH50-2	68.8	26.1	47	66.8	21.3	52	201	10.5	2.57	36	426	3.01E+07	1570	6.7	800	804	0.99
20	Z200D-TH100-1	69.7	22.6	47	70.1	26.7	53	201	7.6	2.57	28	427	3.10E+07	1607	6.7	720	839	0.86
21	Z200D-TH100-2	69.6	25.2	46	70.8	28.5	54	203	6.9	2.59	53	421	3.19E+07	3046	6.7	960	1041	0.92
22	Z200B-TH25-1	70	26.2	46	70.3	27.8	53	204	6.1	2.54	42	421	2.96E+07	1200	6.7	870	719	1.21
23	Z200B-TH25-2	68.9	26.6	46	68.1	26.7	53	204	6.5	2.54	32	420	2.91E+07	929	6.7	650	641	1.01
24	Z200B-TH50-1	72.1	25.1	48	71.4	28	53	203	7.5	2.57	47	424	3.10E+07	1956	6.7	1010	878	1.15
25	Z200B-TH50-2	68	25.2	47	68.7	26.8	53	206	7.7	2.57	40	424	3.06E+07	1765	6.7	910	877	1.04
26	Z200B-TH100-1	68.1	26	47	68.7	25	52	202	6.7	2.57	34	421	3.03E+07	1997	6.7	850	901	0.94
27	Z250D-TH25-1	68.4	20.1	54	73.9	20.8	47	253	6.5	1.5	39	404	5.46E+06	1140	6.7	470	424	1.11
28	Z250D-TH25-2	67.7	18.7	55	72.6	20.2	47	254	5.6	1.5	36	409	5.41E+06	1064	6.7	460	426	1.08
29	Z250D-TH50-1	67.2	21.1	54	71.9	20.7	47	252	6.5	1.54	28	405	5.87E+06	1250	6.7	430	450	0.96
30	Z250D-TH50-2	71.9	20.1	56	72.9	20.6	47	253	6.3	1.54	30	402	5.80E+06	1252	6.7	460	437	1.05
31	Z250D-TH100-1	71.9	21.9	55	71.6	19.9	48	257	6.9	1.52	44	397	5.48E+06	2448	6.7	560	460	1.22
32	Z250D-TH100-2	72	22	54	73	20	46	253	6.1	1.52	31	409	5.54E+06	1722	6.7	430	446	0.96
33	Z250B-TH25-1	74.7	22	55	70.2	21.5	47	254	6	1.5	27	402	5.23E+06	723	6.7	410	353	1.16
34	Z250B-TH25-2	69.3	20.4	55	72.5	20.1	47	258	6.2	1.52	39	398	5.56E+06	1126	6.7	530	428	1.24
35	Z250B-TH50-1	69.4	19.1	55	71.2	20.5	48	253	5.9	1.52	41	398	5.56E+06	1772	6.7	560	459	1.22
36	Z250B-TH50-2	68	19.4	55	70	19.8	48	254	5.7	1.52	39	402	5.52E+06	1721	6.7	530	462	1.15
37	Z250B-TH100-1	68	18	53	72.9	20	45	254	5.1	1.52	37	388	5.63E+06	2176	6.7	510	477	1.07
38	Z250B-TH100-2	68.1	22.6	54	72.8	20.2	47	254	6.8	1.52	40	409	5.62E+06	2349	6.7	540	477	1.13
39	C200D-TH25-1	63.8	21	90	64.5	21	90	203	4.8	2.57	20	525	5.38E+07	627	6.7	460	577	0.80
40	C200D-TH25-2	66.8	20.3	90	64.4	20.9	90	203	4.6	2.57	26	526	5.28E+07	778	6.7	510	610	0.84
41	C200D-TH50-1	61.5	21.2	90	62.8	20.2	90	203	4	2.58	21	514	5.41E+07	1024	6.7	560	733	0.76
42	C200D-TH50-2	62.3	20.1	90	68	21.7	90	203	5.8	2.57	24	531	5.60E+07	1156	6.7	650	797	0.82
43	C200D-TH100-1	64.7	21.2	90	65.7	21	90	203	6.3	2.57	26	541	5.44E+07	1607	6.7	820	832	0.99
44	C200D-TH100-2	64.4	21.3	91	64.9	21.1	91	203	4.6	2.57	12	547	5.38E+07	745	6.7	540	597	0.90
45	C250D-TH25-1	63.1	21.2	90	63.2	20.9	90	254	4.3	1.49	22	411	9.28E+06	697	6.7	290	326	0.89
46	C250D-TH25-2	62.9	20.9	89	64.4	20.3	89	254	4.3	1.5	33	410	9.56E+06	1049	6.7	380	391	0.97
47	C250D-TH50-1	63.1	20.1	90	68.1	21.3	90	254	4.8	1.5	22	413	9.89E+06	1046	6.7	300	371	0.81
48	C250D-TH50-2	63.1	21.1	90	68.8	19	90	254	5.6	1.5	12	413	9.88E+06	571	6.7	220	296	0.74
49	C250D-TH100-1	64.1	19.7	89	65.2	18.9	89	254	4.4	1.5	22	417	9.51E+06	1373	6.7	320	390	0.82
50	C250D-TH100-2	62.7	20.7	91	65	18	91	254	4.8	1.5	30	413	9.49E+06	1914	6.7	420	432	0.97